Journal of Applied Polymer Science

Influence of Silanized Low-Dimensional Carbon Nanofillers on Mechanical, Thermomechanical, and Crystallization Behaviors of Poly(L-lactic acid) Composites—A Comparative Study

Wenxiao Li, Chengbo Shi, Mingjing Shan, Qiwei Guo, Zhiwei Xu, Zhen Wang, Caiyun Yang, Wei Mai, Jiarong Niu

Key Laboratory of Advanced Braided Composites, Ministry of Education, Department of Nonwoven, School of Textiles, Tianjin Polytechnic University, Tianjin, 300160, China

Correspondence to: Z. Xu (E-mail: xuzhiwei@tjpu.edu.cn).

ABSTRACT: Composites were investigated regarding the comparison of multi-walled carbon nanotubes (MWCNTs) with exfoliated graphene(EG) in poly(L-lactic acid) (PLLA) and the effect of silane-treated carbon nanofillers on properties of PLLA composites. Solution blending method was used to prepare PLLA composites at a filler content of 0.5 wt %. Fourier transform infrared spectroscopy and X-ray photoelectron spectra results indicated the attachment of silane molecules on the surface of these nanofillers. It was found that the addition of these nanofillers greatly enhanced the mechanical, thermomechanical, and crystallization behaviors of PLLA due to the heterogeneous nucleation effect. Moreover, the silane-treated fillers further enhanced the breaking elongation moderately (although the materials are still brittle), modulus and thermal property of the nanocomposites, without sacrificing the tensile strength, compared with the pristine nanocomposites. On the other hand, composites reinforced with MWCNTs and EG perform almost the same mechanical property. And EG outperformed MWCNTs in thermomechanical properties of composites when being used as the reinforcement of PLLA. Conversely, composites reinforced with MWCNTs showed better crystallization properties than those reinforced with EG. Interestingly, no significant changes were observed for the crystallization properties of PLLA composites when MWCNTs and EG had been treated by silane coupling agent. © 2013 Wiley Periodicals, Inc. J. Appl. Polym. Sci. 130: 1194–1202, 2013

KEYWORDS: biopolymers and renewable polymers; nanotubes; graphene and fullerenes; mechanical properties; crystallization

Received 26 November 2012; accepted 9 March 2013; Published online 19 April 2013

DOI: 10.1002/app.39259

INTRODUCTION

Biodegradable and biocompatible poly(L-lactic acid) (PLLA) has received much more attention recently. Because of its good mechanical properties, nontoxic to the human body and the environment, as well as versatile fabrication processes, PLLA has excellent potential for substitution of petroleum-based polymers.[1–6] However, some disadvantages such as relatively poor mechanical properties, slow degradation rate and slow crystallization rate have limited its wide practical application. Therefore, polymer blending and nanocomposite preparation have often been employed to modify the physical properties of PLLA in order to extend its practical application.[7–11]

Polymers reinforced with nanosized fillers are promising candidates for various applications requiring lightweight, high-performance, and multifunctional materials. To date, pristine clays,[12] organically modified clays,[13,14] nanofibers,[15] whiskers,[16] or more recently carbonaceous fillers[3,17,18] have received much more attention. Among conventional nanofillers, both carbon nanotubes (CNTs) and graphene have exceptional electric transport, thermal and mechanical properties, which appear as excellent candidates to make advanced functional composite materials.[19] Therefore, comprehensive studies have been performed in terms of nanocomposites reinforced with CNTs and graphene. Wu et al.[20] prepared the PLLA/MWCNTs hybrids via melt blending method and the results demonstrated a dramatic enhancement in thermal properties of PLLA. Kim and Jeong[21] prepared a series of PLLA/exfoliated graphite nanocomposites at different exfoliated graphite loadings by melt compounding, and found that thermal stability, mechanical and electrical properties have been improved in the nanocomposites at small exfoliated graphite loadings. Although MWCNTs and EG are both nanosized carbon materials, EG have a layered structure instead of tubular structure of CNTs, leading to different performance in composites.[22] Several scientific studies could be found on the potential of various carbon-based nanofillers in increasing both mechanical and thermal properties of polymer matrices. However, little work has been done on the comparison of CNTs and

graphene on mechanical, thermal, and crystallization behaviors of PLLA nanocomposites.

Also, these nanofillers have inert surfaces and tend to agglomerate in organic solvents, making further processing difficult, or even impossible. Given the dissimilar surface chemistry of carbonaceous fillers and polymer, several attempts have been conducted to modify the surface of carbonaceous fillers to improve their bonding to polymer.[23,24] One of these is an oxidative method utilizing strong acids, such as H_2SO_4 and HNO_3, by which hydroxyl and carboxylic acid moieties are created on nanofillers.[25,26] The silanization of functionalized nanotubes is another preferred method used to enhance the interfacial adhesion between nanotubes and the matrix.[27–31] But the studies focusing on the influence of silanization on properties of PLLA/various nanofillers are relatively few and not thorough enough.

In the present study, a series of PLLA nanocomposites containing different low-dimensional carbonaceous fillers were prepared, with constant filler content 0.5 wt % in every case, as in most cases, a filler content of 0.5% leads to optimum properties.[32] The fillers include pristine multi-walled carbon nanotubes (p-MWCNTs), silanized multi-walled carbon nanotubes (s-MWCNTs), pristine exfoliated graphene (p-EG) and silanized exfoliated graphene (s-EG). We confirmed the success of grafted chains on MWCNTs and EG by Fourier transform infrared spectroscopy (FTIR) and X-ray photoelectron spectra (XPS) measurements. And various performances of PLLA and its composites were characterized by tensile tests, field emission scanning electron microscopy (FE-SEM), dynamic thermomechanical analysis (DMA), and differential scanning calorimetry (DSC).

EXPERIMENTAL

Materials

PLLA was purchased from Ningbo Global Biological Material. Graphite was provided by Nanjing XF Nanomaterial Science and Technology, China. MWCNTs were obtained from Nanjing XF Nanomaterial Science and Technology. The diameter is around 10–50 nm, and the length is within 1–30 μm. 3-Aminopropyltriethoxy silane (APTES) with purity of 95% (supplied by Tianjin Chemical Reagent No.1 Plant) was used as the silane functionalization agent.

Processing of Nanocomposites

Exfoliation of Graphite Oxide. Graphite oxide (GO) was prepared according to the improved Hummers' method.[33] Thermal exfoliation of GO as prepared above was achieved by placing GO (200 mg) into a 25 mm inside diameter, 20 cm long quartz tube that was sealed at one end. The quartztube was quickly inserted into the tube furnace preheated to 1050°C and held for 30 s. The sudden increase in temperature(~2000°C /min) resulted in exfoliation of GO to graphene.

Silanization of MWCNTs and EG. Taking MWCNTs as an example, 3.5 mL of 1.75 wt % APTES was added into a mixture (~250 mL) of ethanol and water (9:1, mass ratio), and then the mixture was hydrolyzed 3 h at room temperature. 1 g of MWCNTs was added into a three-neck flask with the mixture and dispersed through ultrasonication (in water bath) for 30 min. After the reaction, the mixed solution was under backflow at 70°C for 3 h. The product was obtained by filtration and washing with water. The silane-treated MWCNTs were further dried in a vacuum oven at 80°C for 24 h. EG was also modified according to the above procedure. The obtained samples were named s-MWCNTs and s-EG.

Fabrication of Composites. Solution blending was utilized to prepare neat PLLA and its nanocomposites. For neat PLLA, 5 g PLLA particles were dissolved in 50 mL chloroform and sonicated in an ultrasonic bath for 1 h to dissolve PLA completely. For preparation of PLLA nanocomposites, the nanofiller content was 0.5 wt %. In case of PLLA/p-MWCNTs composites, the detailed experimental procedure was described as follows: First, the MWCNTs were added into the chloroform at a concentration of 0.5 mg/mL. The mixture was further sonicated with an ultrasonic generator for 2 h to make a uniformly dispersed suspension. Second, PLLA was placed into the mixture and stirred for 1 h to dissolve the PLLA. Finally, the mixture of PLLA and p-MWCNTs was further sonicated for 2 h. Through the aforementioned procedure, PLLA was mixed with p-MWCNTs. Other composites were all prepared as mentioned above. All solutions of neat PLLA and its composites were poured into a dish to evaporate the solvent at room temperature for 24 h. The residual solvent was removed by placing the composites in a vacuum oven at 70°C for 24 h. For brevity, they were abbreviated as PLLA/p-MWCNTs, PLLA/s-MWCNTs, PLLA/p-EG, and PLLA/s-EG.

Characterization

Transmission electron microscopy (TEM) observations of p-MWCNT and s-MWCNTs were performed using a Hitachi 7650 operated at 200 kV. Atomic force microscopic (AFM) measurements with the typical contact-mode were performed using Digital Instrument CSPM5500. Fourier transform infrared spectroscopy (FTIR) analyses were performed on nano-samples using a Bruker Tensor 27 system. The spectra were recorded from 500 to 4000 cm^{-1} with a resolution of 2 cm^{-1} and 32 scans. XPS measurements were performed using a PHI 5700 ESCA System Auger electron spectrometer (Physical electronics company, America) equipped with a hemispherical electron analyzer and a scanning monochromatic Al Kα ($h\nu$=1486.6 eV) X-ray source.

The tensile tests were performed using a universal testing machine, YG028, Wenzhou fangyuan instrument China, with a load cell of 10 kN and with a crosshead speed of 2 mm/min. The elastic modulus was calculated from the initial part of the slope from stress–strain curves. At least five test samples were tested for each material and the average values are presented. For morphological observation, the composite films were frozen in liquid nitrogen, and then quickly fractured. The fracture surfaces were observed using a field emission SEM (Hitachi S-4800) operated at an acceleration voltage of 10.0 kV. The samples were sputter-coated with gold to avoid charging. The dynamic mechanical properties of nanocomposites were carried out using the dynamic mechanical analyzer, DMA Q800 TA Instruments (New Jersey, USA), in tensile mode. The measurements were performed at a constant frequency of 1 Hz with a temperature range from 30°C to 160°C at a heating rate of

3°C/min. The test specimen dimensions were ~0.1×10.0×30.0 mm. The presented data were based on five measurements. Melt rheology tests of these nanocomposites were performed on a Rheograph 25 (Goettfert) with a *L/D* (20 mm/1 mm)die at 200°C.The apparent melt viscosity for each material was determined at apparent shear rate of 150, 225, 337.5, 506.3, 759.4, 1139.1, 1708.6, 2562.9, 3844.3, 5766.5 s^{-1}. A rheology curve was plotted for each material of apparent viscosity versus shear rate.

Thermal characterization of PLLA and composites was performed with a DSC 7 Perkin-Elmer instrument calibrated with indium under nitrogen atmosphere. Aluminum sample pans with ~3 mm diameter were used for all samples. The test samples were heated from 40 to 180°C at the rate of 10°C/min and held for 5 min at 180°C to eliminate the previous thermal history. They were then cooled to 40°C at 20°C /min and subsequently scanned from 40 to 180°C at 10°C/min again. All the runs were under nitrogen atmosphere.

RESULTS AND DISCUSSION

Characterization of MWCNTs and EG

Presently, TEM is an effective method to attain qualitative information of nanofillers.[34] In Figure 1, representative TEM micrographs for the investigation of p-MWCNTs and s-MWCNTs are shown. As it can be seen from Figure 1(a,b), both the p-MWCNTs and s-MWCNTs are relative lucid and the diameters of them are not uniform. In addition, we can see that the tips of s-MWCNTs are seemly coated with something, which may preliminarily be regarded as silane.

AFM measurement is the most used method to validate the structure of modified single graphene sheet with size in microscale. We measure the thicknesses of at least five sheets for both s-EG and p-EG. Figure 2(a,b) shows the representative contact mode AFM images of p-EG and s-EG sheets, respectively. The grafted chains on two sides of graphene sheets heighten its thickness to about 2.2±0.16nm, comparing to the thickness of p-EG about 1.5 ± 0.20 nm. The result reveals that the APTES chains were likely to attach onto the surface of EG.

To validate the very existence of grafted APTES chains, we used FTIR to characterize MWCNTs and EG, as shown in Figure 3. Figure 3(a) shows the FTIR results of the MWCNTs. For pristine MWCNTs, the band at 1384 cm^{-1} is attributed to the presence of hydroxyl group(-OH) on the surface of the MWCNTs, which is believed to result from either ambient atmospheric moisture bound to the MWCNTs or oxidation during purification of the raw material.[35] In the spectrum of s-MWCNTs, the broad band around 3423 cm^{-1} is assigned to the hydrogen-bonded amide group(-NH_2) of APTES, whereas the band around 1548 and 1627 cm^{-1} are assigned to the combination of bending of the N-H bond and stretching of the C-N bond in the amide group. Additionally, signal corresponding to Si-O stretch can be seen at 1101 cm^{-1}.

Figure 3(b) shows the FTIR spectrum of EG. Pristine EG also showed -OH stretch at 1383 cm^{-1}. For the silanized EG, the -NH_2 of at 3423 cm^{-1} also can be seen. On the other band, two new bands at 2918 and 2854 cm^{-1} associated with the

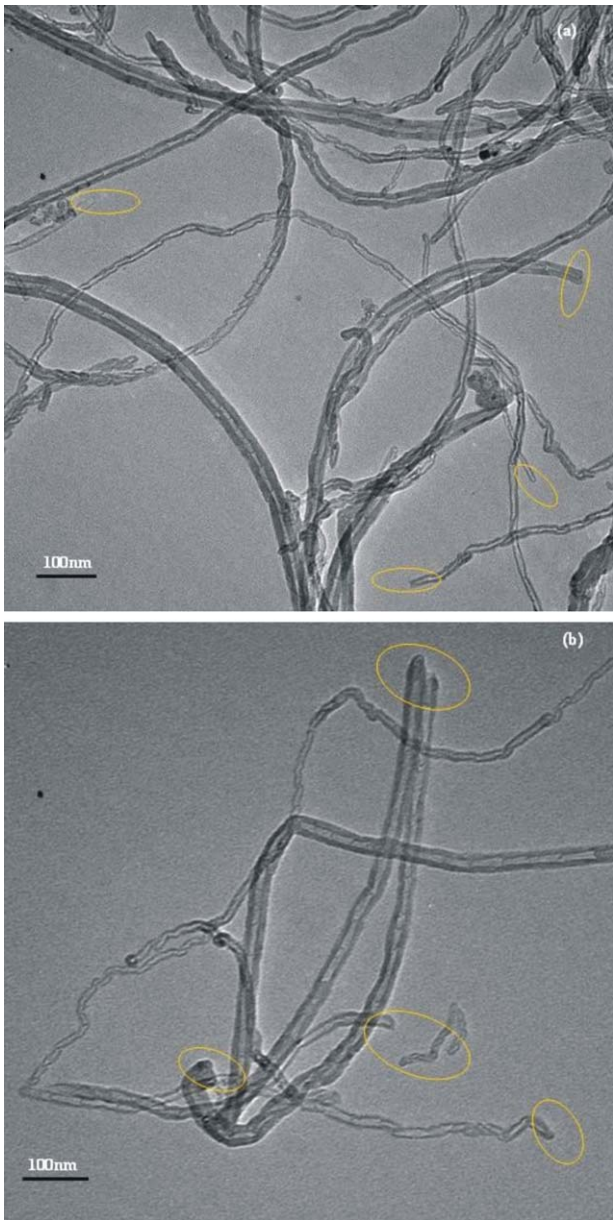

Figure 1. TEM micrographs of (a) p-MWCNTs and (b) s-MWCNTs. [Color figure can be viewed in the online issue, which is available at wileyonlinelibrary.com.]

stretching of the methylene groups(-CH_2) from the APTES molecules appeared. Additionally, signals corresponding to C-N and Si-O stretches can be seen at 1633 and 1068 cm^{-1}, respectively. The appearance of new absorption peaks confirm that the APTES molecules are successfully attached onto the surface of MWCNTs and EG.

In addition, XPS was also conducted to confirm the attachment of silane on MWCNTs and EG. Figure 4 shows the survey spectra of p-MWCNTs, p-EG, s-MWCNTs, and s-EG. The spectrums of p-MWCNTs and p-EG consist mainly of two components, namely C1s core-level spectra (285 eV) and O1s core-level spectra (532.2 eV), as shown in Figure 4(a,b). After the fillers was treated with silane modifier, Si2p core-level spectra (103.5 eV)

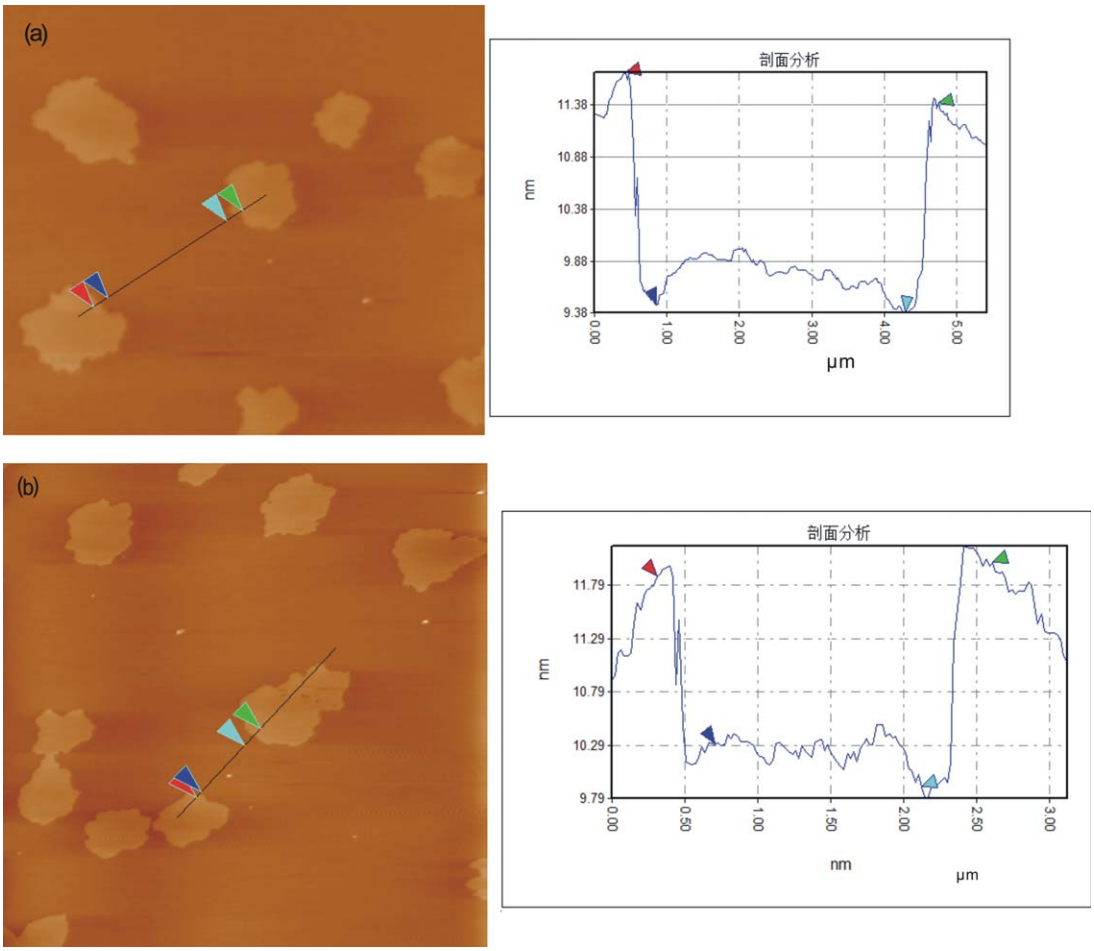

Figure 2. Contact mode AFM images of (a) p-EG and (b) s-EG with height profiles. The samples were prepared by drop-casting corresponding dilute dispersions onto mica sheets. [Color figure can be viewed in the online issue, which is available at wileyonlinelibrary.com.]

and N1s core-level spectra (399.4 eV) appear on the survey spectra, representative peaks are shown in Figure 4(c,d).

Furthermore, the attachment ratio of the silane on the low-dimensional carbon nanofiller surface was determined by elemental analysis from the difference of silicon content (Si, wt %) after and before treatment, using eq. (1):

$$W_{\mathrm{APTES}}\,(\mathrm{wt}\,\%) = \frac{W_{\mathrm{Si}} \times M_{\mathrm{APTES}}}{M_{\mathrm{Si}}}\,\% \qquad (1)$$

where W_{APTES} and W_{Si} designate the weight percent of APTES content and silicon content in the silanized nanofillers, respectively. M_{APTES} and M_{Si} are respectively the molecular weight of APTES and silicon (M_{APTES} = 231 g/mol, M_{Si} = 28 g/mol). Table I shows the weight percentages of C, O, N, Si. Assuming the attached and grafted chains were completely APTES, the weight percentage of silane molecules attached to the MWCNTs and EG are 39.4 wt % and 42.3 wt %, respectively, as calculated according to eq. (1).

Characterization of Nanocomposites

Tensile Characteristics. Generally, the addition of nanofillers into polymer matrices is expected to result in improved properties such as better tensile and flexural strength, higher modulus, and dimensional stability, etc. The typical tensile stress–strain curves of neat PLLA compared with composites containing different nanofillers are shown in Figure 5 and the corresponding results are summarized in Table II. Neat PLLA shows a lowest tensile strength of 32.3 MPa, an elongation at break of 2.3%, and a modulus of 2.2 GPa. This can be explained by the fact that MWCNTs and EG have heterogeneous nucleation effect on PLLA matrix. As shown in Table II, on the one hand, composites reinforced with MWCNTs (including pristine MWCNTs and silanized MWCNTs) offered almost the same tensile strength and breaking elongation compared with those reinforced with EG (including pristine EG and silanized EG) if standard deviations are considered. EG was more likely to aggregate than MWCNTs due to its high specific surface area, which could explain why EG has a higher contact area with PLA theoretically but the addition of EG did not enhance the strength of composite when compared with CNTs. On the other hand, the tensile strength of PLLA/silanized filler composites is also similar to those of PLLA/pristine filler composites. Nevertheless, the elongations at break of PLLA/silanized filler composites are nearly double for the neat PLLA and greater than PLLA/pristine filler composites, and increase to 4.8% and 4.0%, respectively. The elongations at break of PLLA/silanized filler

Applied Polymer SCIENCE

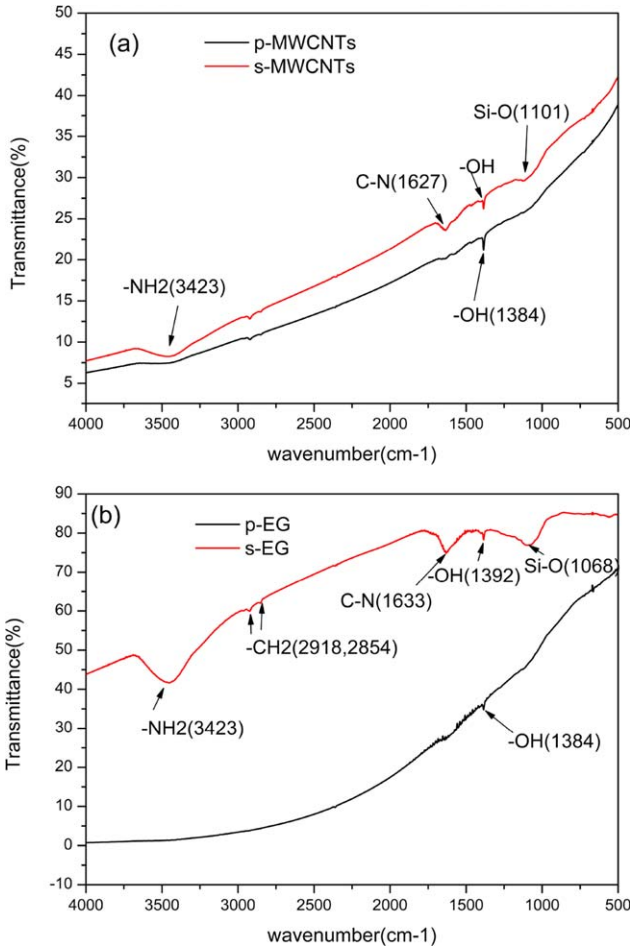

Figure 3. FTIR spectra of (a) p-MWCNTs and s-MWCNTs, (b) p-EG and s-EG. [Color figure can be viewed in the online issue, which is available at wileyonlinelibrary.com.]

composites increase obviously although the materials are still brittle. It is mainly because silane modifiers enhance the interfacial adhesion between nanofillers and the PLLA.

As seen in Table II, the incorporation of carbonaceous fillers improves the modulus of PLLA, signifying that stress transfers from the polymeric matrix to stiffer fillers occurred. The modulus of PLLA increases by 10.9%, 47.9%, 23.7%, and 53.4% at contents of 0.5 wt % p-MWCNTs, s-MWCNTs, p-EG, and s-EG, respectively. In particular, addition of EG and MWCNTs do not exhibit obvious difference in Young's modulus of composites. This may explained by the fact that EG and MWCNTs have similar chemical structure. Although EG has higher specific surface area than MWCNTs, it is more inclined to occur stacking in the process of manufacturing composite due to its layer structure, consequently, impairing its theoretical reinforcing effect.[36] So it is still a challenging work to obtain the complete exfoliated structure of EG. In addition, the silane modification of MWCNTs and EG significantly increase Young's modulus of composites, due to the enhanced interfacial adhesion between nanofillers and the PLLA. These results demonstrated that the EG need to be further researched to realize its advantages, and the silane coupling agent is in favor of the interaction between PLLA and carbonaceous fillers.

Nanocomposite Morphology. Assessment of the dispersion state of nanofillers in the polymer matrix and the interfacial adhesion between two phases is essential to understand the nanocomposite behavior. Figure 6 shows the FE-SEM micrographs of the fracture surfaces of neat PLLA and nanocomposites. For the p-MWCNTs/PLLA nanocomposite, severe aggregation of p-SWCNTs and poor interfacial interactions are observed in Figure 6(b). It is seen from Figure 6(c) that the individual s-SWCNTs are randomly dispersed in the matrix, and no apparent MWCNTs aggregation is observed. The results indicate that the morphology of s-SWCNTs/PLLA nanocomposite is different from the p-SWCNTs/PLLA, attributing to the good dispersion of s-MWCNTs in PLLA matrix and the strong interfacial interactions between PLLA and s-MWCNTs. These may be responsible for the enhanced elongation, modulus and thermal property of composites. While we can't distinguish EG in the PLLA matrix due to the two-dimensional structure of it. But we can see the existence of defects such as voids in the fracture surfaces of p-EG/PLLA [Figure 6(d)] which is not obvious in the s-EG/PLLA [Figure 6(e)].

Dynamic Mechanical Analysis. Figure 7 shows the storage modulus (E') and damping factor (tan δ) versus temperature for neat PLLA and its nanocomposites. In Figure 7(a), the storage modulus gradually increased in the order of neat PLLA, PLLA/p-MWCNTs, PLLA/s-MWCNTs, PLLA/p-EG, and PLLA/s-EG composites. Specifically, PLLA reinforced with EG exhibit significantly higher storage modulus compared with those reinforced with MWCNTs. This could be attributed to the fact that EG has a layered structure instead of tubular structure of MWCNTs and posses higher specific surface area. It is noted that PLLA/silanized filler composites exhibit higher storage modulus than PLLA/pristine filler, which can be ascribed to the reinforcing effect of the silanized filler that proved to be finely distributed and dispersed within the PLA matrix.[37] Figure 7(b) shows tan δ of neat PLLA and its nanocomposites as a function of temperature. Tan δ is the ratio of the loss modulus to the storage modulus or the ratio of the energy dissipated to the energy stored during a dynamic loading cycle. The magnitude of the tan δ peak is associated with the damping property of a composites material.[38,39] After introduction of nanofillers(except the p-MWCNTs) to PLLA, the tanδ peak of the nanocomposites became weaker and broader, indicating that the nanocomposites become harder.[40] The abnormal variation of p-MWCNTs/PLA may be ascribed to the severe aggregation of MWCNTs. Furthermore, due to the silane functionalization, a strong interfacial bond and good dispersibility reduce the mobility of the polylactic acid molecules around the CNTs and EG, thus, resulting in increased thermal stability, as seen the increase of glass-transition temperature in Figure 6(b).

Rheological Properties of PLA Nanocomposites. The results obtained from the rheology tests of polymer and carbon nanofillers reinforced polymer is presented in Figure 8. In general, apparent viscosity decreases with the increase of shear rate and the addition of fillers increases the viscosity of PLA. In addition,

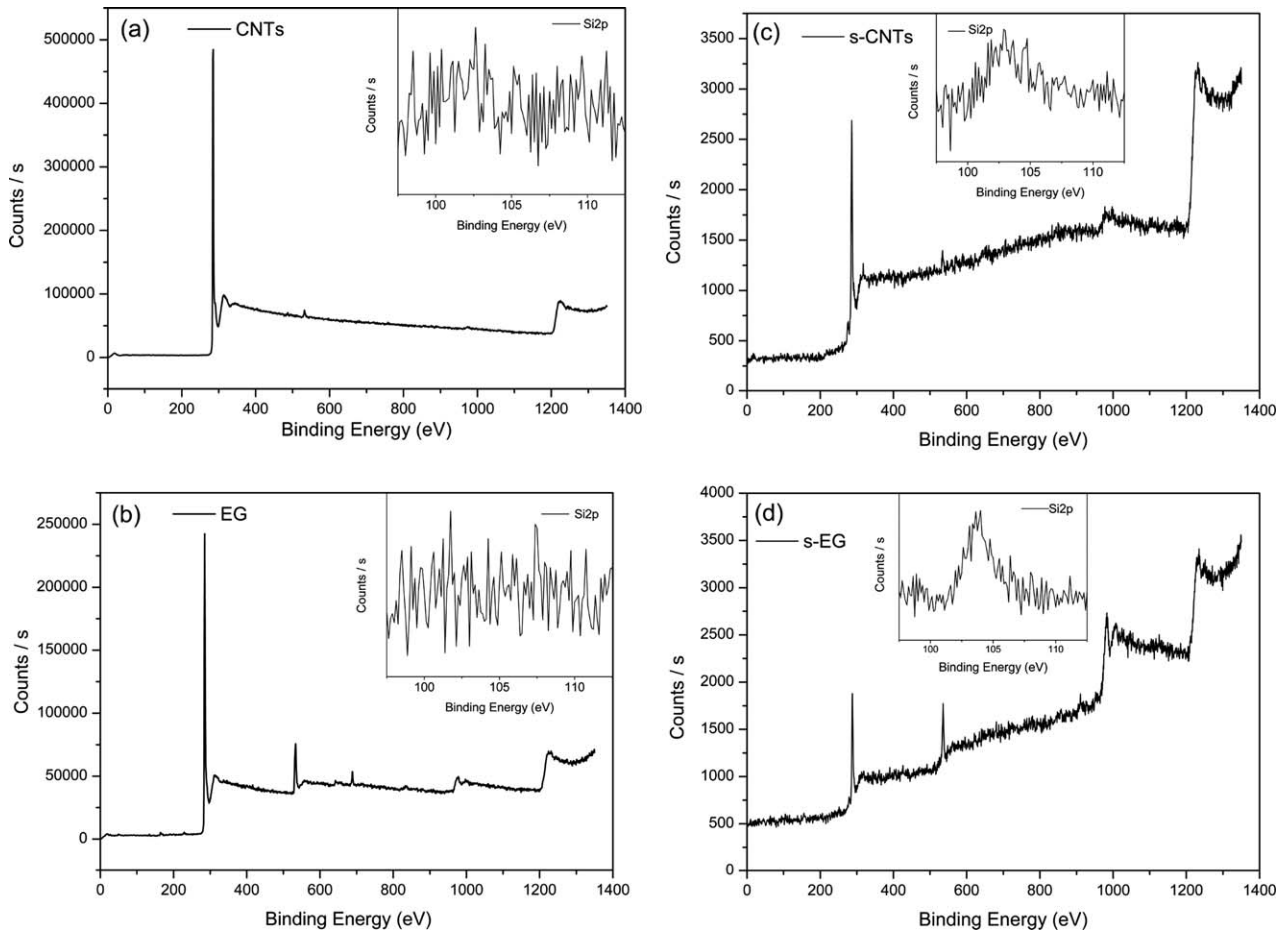

Figure 4. The survey spectra of (a) p-MWCNTs, (b) p-EG, (c) s-MWCNTs, and (d) s-EG.

the viscosity of silanized composites is slightly increase than the pure. This indicates the strong interfacial bond between the fillers and matrix which reduces the mobility of the polylactic acid molecules.

Crystallization Behavior. In the cooling scans [Figure 9(a)], the exothermic peaks with very low intensity are observed for pure PLLA and EG/PLLA, indicating a rather low crystallization capability. As for the two MWCNTs/PLLA nanocomposites, the crystallization peaks have relatively higher intensity and started from higher temperature as a result of enhanced crystallizability. The incorporation of MWCNTs enhances the isothermal melt crystallization of the PLLA matrix. This could be ascribed to the perfect crystal structure of MWCNTs which have nucleating effect to the PLLA.[41]

Figure 9(b) shows the subsequent melting behavior of neat PLLA and its nanocomposites after cooling from the melt at

Table I. Elemental Analysis Data of p-MWCNTs, p-EG, s-MWCNTs, and s-EG

Sample	C1s (wt %)	O1s (wt %)	Si2p (wt %)	N1s (wt %)
p-MWCNTs	98.2	1.7	-	-
p-EG	89.7	8.7	-	-
s-MWCNTs	83.3	8.4	4.8	3.4
s-EG	75.6	15.7	5.1	3.6

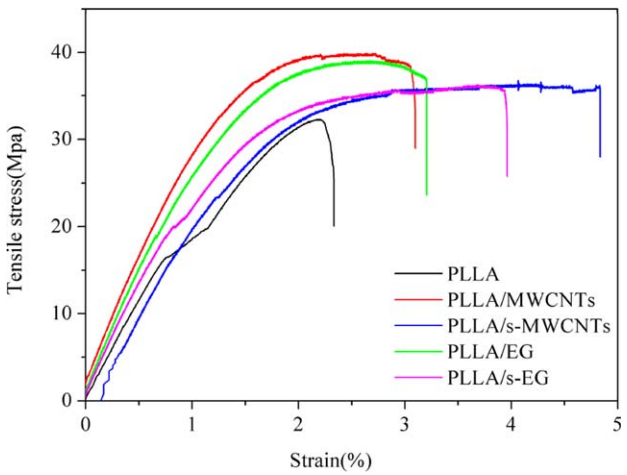

Figure 5. Tensile stress–strain curves of neat PLLA and nanocomposites. [Color figure can be viewed in the online issue, which is available at wileyonlinelibrary.com.]

Table II. Static Mechanical Properties of Neat PLLA and Its Composites

Sample	Tensile strength (MPa)	Elongation at break (%)	Tensile modulus (GPa)
neat PLLA	32.3 ± 2.5	2.3 ± 0.1	2.2 ± 0.2
PLLA/p-MWCNTs	39.8 ± 2.1	3.1 ± 0.2	2.4 ± 0.2
PLLA/s-MWCNTs	36.7 ± 2.0	4.8 ± 0.2	3.2 ± 0.3
PLLA/p-EG	38.9 ± 2.6	3.2 ± 0.1	2.7 ± 0.2
PLLA/s-EG	35.3 ± 2.3	4.0 ± 0.3	3.4 ± 0.3

10°C /min (second heating). Both neat PLLA and its nanocomposites exhibit the glass transition temperatures of around 62°C. However, neat PLLA and PLLA/EG composites show a cold crystallization peak temperature of about 105°C with crystallization enthalpy being 35.4 J/g. But PLLA/MWCNTs composites do not show cold crystallization at all. The melting endotherms locate at around 167.8°C for both neat PLLA and its nanocomposites. The values of heat of fusion ($\triangle H_m$) are around 34.8 J/g for neat PLLA and increase to 39.6, 41.0, 40.0, and 41.2 J/g for p-MWCNTs, s-MWCNTs, p-EG, and s-EG composites, respectively. On the basis of the heat of fusion of

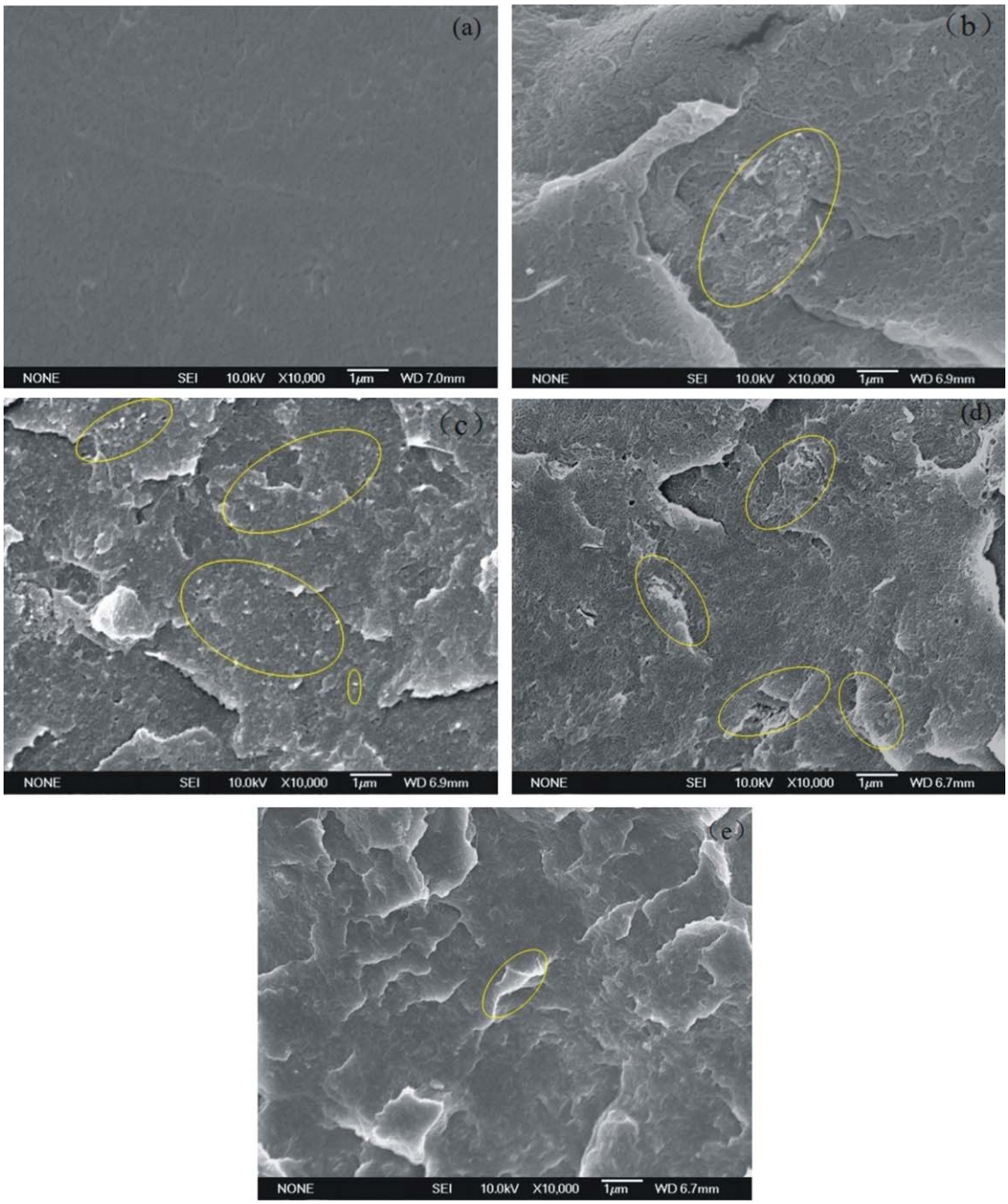

Figure 6. FE-SEM images of the fractured surface of (a) PLLA, (b) PLLA/p-MWCNTs, (c) PLLA/s-MWCNTs, (d) PLLA/p-EG, and (e) PLLA/s-EG, respectively. [Color figure can be viewed in the online issue, which is available at wileyonlinelibrary.com.]

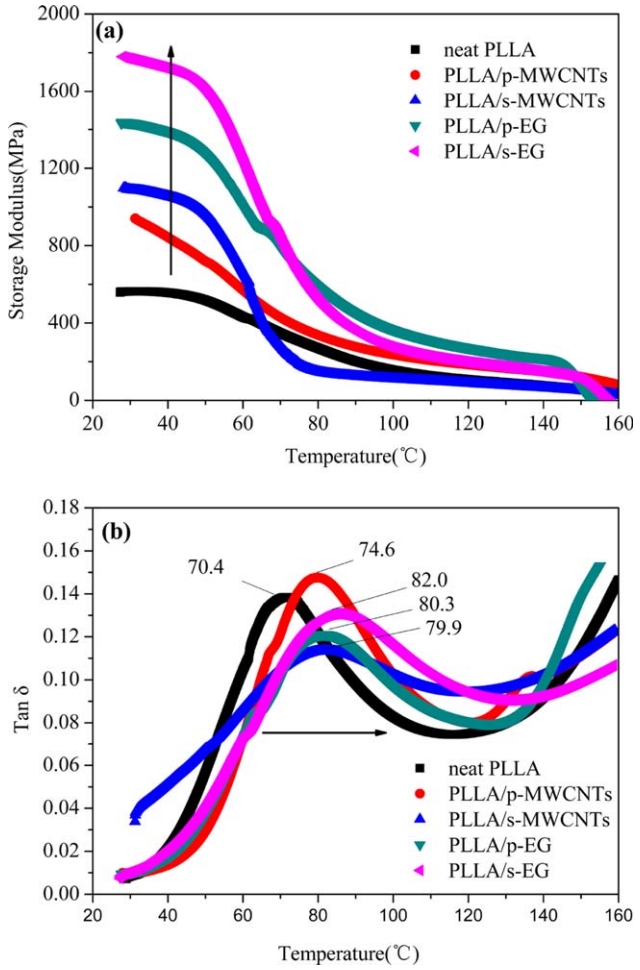

Figure 7. DMA analysis of PLLA and PLLA nanocomposites: (a) storage modulus and (b) tan δ curves. [Color figure can be viewed in the online issue, which is available at wileyonlinelibrary.com.]

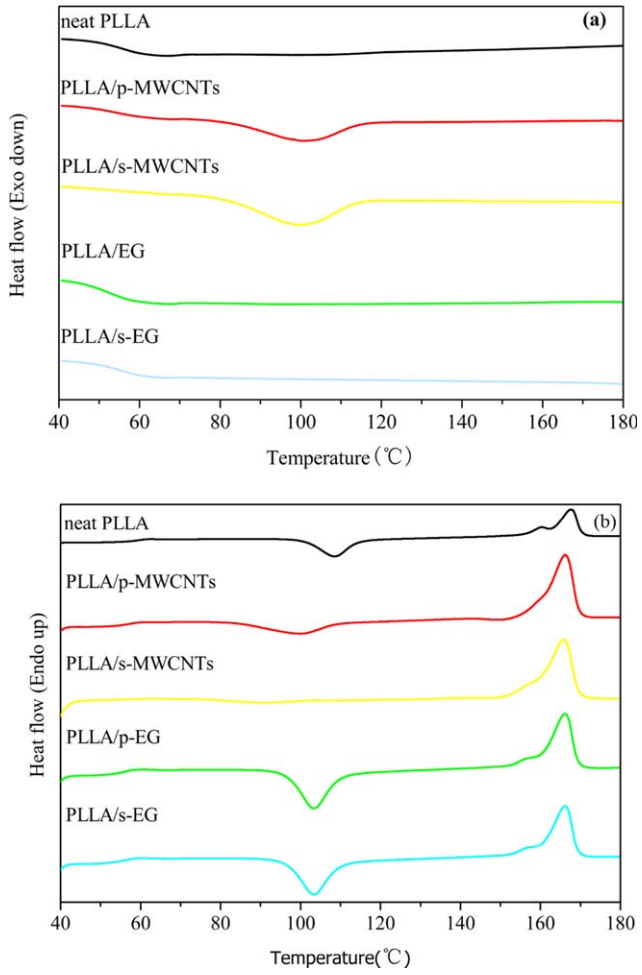

Figure 9. DSC thermograms of neat PLLA and its nanocomposites: (a) first cooling and (b) second heating. [Color figure can be viewed in the online issue, which is available at wileyonlinelibrary.com.]

100% crystalline ($\triangle H_{0m}$) PLLA (93.1 J/g), the values of degree of crystallinity (W_c) are determined to be 37.3%, 42.6%, 43.9%, 42.9%, and 44.2% for neat PLLA, PLLA/p-MWCNTs, PLLA/s-MWCNTs, PLLA/p-EG, and PLLA/s-EG, respectively. This shows that the silanization of nanofilles had little influence on the crystallization behavior of the nanocomposites.

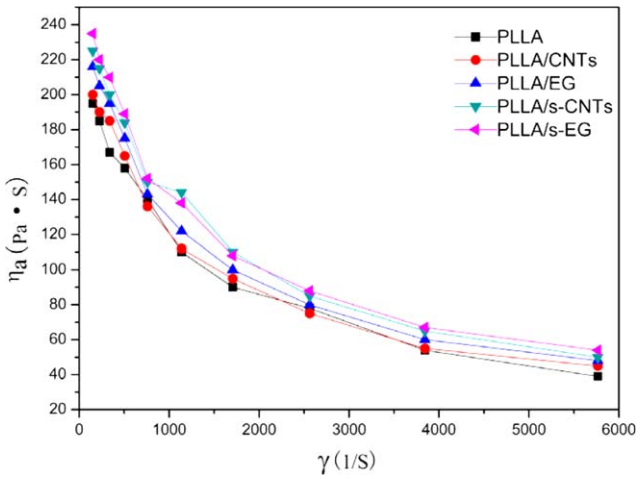

Figure 8. The viscosity at different shear rates of neat PLLA and PLLA nanocomposites. [Color figure can be viewed in the online issue, which is available at wileyonlinelibrary.com.]

CONCLUSIONS

Nanocomposites consisting of poly (L-lactic acid) resin and different types of carbon nanofillers were produced by solution blending. The composites were investigated by comparison of MWCNTs and EG in PLLA and the effect of silane-treated carbonaceous filler on properties of PLLA nanocomposites.

The results revealed that the APTES chains were successfully attached to the carbonaceous filler surfaces. In general, composites reinforced with MWCNTs offered superior crystallization property compared with those reinforced with EG. However, EG and MWCNTs performed similar behaviors in tensile strength, breaking elongation, Young's modulus and thermomechanical properties. In addition, the silane modification of MWCNTs and EG significantly increase breaking elongation, Young's modulus and storage modulus of composites without sacrificing the tensile strength of the pristine nanocomposite.

The DSC results also show that there is not a significant change in crystallization properties of PLLA/silanized filler composites.

ACKNOWLEDGMENTS

The authors acknowledge support from the National Natural Science Foundation of China (11175130), Natural Science Foundation of Tianjin, China (10JCYBJC02300) and China Postdoctoral Science Foundation (2012M520578).

REFERENCES

1. Zhao, Y.; Qiu, Z.; Yang, W. *Compos. Sci. Technol.* **2009**, *69*, 627.
2. Murariu, M.; Dechief, A. L.; Bonnaud, L.; Paint, Y.; Gallos, A.; Fontaine, G.; Bourbigot, S.; Dubois, P. *Polym. Degrad. Stabil.* **2010**, *95*, 889.
3. Papageorgiou, G. Z.; Achilias, D. S.; Nanaki, S.; Beslikas, T.; Bikiaris, D. *Thermochim. Acta* **2010**, *511*, 129.
4. Pan, P.; Liang, Z.; Cao, A.; Inoue, Y. *ACS Appl. Mater. Interfaces* **2009**, *1*, 402.
5. Jiao, L.; Huang, C.-L.; Zeng, J.-B.; Wang, Y.-Z.; Wang, X.-L. *Thermochim. Acta* **2012**, *539*, 16.
6. Suardana, N. P. G.; Ku, M. S.; Lim, J. K. *Mater. Des.* **2011**, *32*, 1990.
7. Wang, H.; Qiu, Z. *Thermochim. Acta* **2011**, *526*, 229.
8. Chen, B.-K.; Shen, C.-H.; Chen, A. F. *Polym. Bull.* **2012**, *69*, 313.
9. Bang, G.; Kim, S. W. *J. Indust. Eng. Chem.* **2012**, *18*, 1063.
10. Yan, S.; Yin, J.; Cui, L.; Yang, Y.; Chen, X. *Colloids Surf. B Biointerfaces* **2011**, *86*, 218.
11. Taccola, S.; Desii, A.; Pensabene, V.; Fujie, T.; Saito, A.; Takeoka, S.; Dario, P.; Menciassi, A.; Mattoli, V. *Langmuir* **2011**, *27*, 5589.
12. Marras, S. I.; Tsimpliaraki, A.; Zuburtikudis, I.; Panayiotou, C. *J. Phys.* **2007**, *61*, 1366.
13. Fukushima, K.; Tabuani, D.; Camino, G. *Mater. Sci. Eng. C* **2009**, *29*, 1433.
14. Balakrishnan, H.; Hassan, A.; Wahit, M. U.; Yussuf, A. A.; Razak, S. B. A. *Mater. Des.* **2010**, *31*, 3289.
15. Wang, B.; Cai, Q.; Zhang, S.; Yang, X.; Deng, X. *J. Mech. Behav. Biomed. Mater.* **2011**, *4*, 600.
16. Nakamura, A.; Iji, M. *J. Mater. Sci.* **2010**, *46*, 1439.
17. Villmow, T.; Pötschke, P.; Pegel, S.; Häussler, L.; Kretzschmar, B. *Polymer* **2008**, *49*, 3500.
18. Rahmanian, S.; Thean, K. S.; Suraya, A. R.; Shazed, M. A.; Mohd Salleh, M. A.; Yusoff, H. M. *Mater. Des.* **2013**, *43*, 10.
19. Du, J.; Zhao, L.; Zeng, Y.; Zhang, L.; Li, F.; Liu, P.; Liu, C. *Carbon* **2011**, *49*, 1094.
20. Wu, C.-S.; Liao, H.-T. *Polymer* **2007**, *48*, 4449.
21. Kim, I.-H.; Jeong, Y. G. *J. Polym. Sci. Part B: Polym. Phys.* **2010**, *48*, 850.
22. Shin, M. K.; Lee, B.; Kim, S. H.; Lee, J. A.; Spinks, G. M.; Gambhir, S.; Wallace, G. G.; Kozlov, M. E.; Baughman, R. H.; Kim, S. *J. Nat. Commun.* **2012**, *3*, 650.
23. Eitan, A.; Jiang, K.; Dukes, D.; Andrews, R.; Schadler, L. *Chem. Mater.* **2003**, *15*, 3198.
24. Gao, Y.; Wang, Y.; Shi, J.; Bai, H.; Song, B. *Polym. Test.* **2008**, *27*, 179.
25. Tan, L.; Chen, Y.; Zhou, W.; Ye, S.; Wei, J. *Polymer* **2011**, *52*, 3587.
26. Hirsch, A. *Angewandte Chemie-Int. Ed.* **2002**, *41*, 1853.
27. Kathi, J.; Rhee, K. Y. *J. Mater. Sci.* **2008**, *43*, 33.
28. Jiang, Z.; JongDae, K.; Haiqing, P.; Margrave, J. L.; Khabashesku, V. N.; Barrera, E. V. *Nano Lett.* **2003**, *3*, 1107.
29. Xing, Y.; Li, L.; Chusuei, C.; Hull, R. *Langmuir* **2005**, 21.
30. Tasis, D.; Tagmatarchis, N.; Bianco, A.; Prato, M. *Chem. Rev.* **2006**, *106*, 1105.
31. Carlos, V.-S.; Ana, L. M.-H.; Witold, B.; Castano, V. M. *J. Nanomater.* **2011**, 2011, 1.
32. Lebovka, N. I.; Lysenkov, E. A.; Goncharuk, A. I.; Gomza, Y. P.; Klepko, V. V.; Boiko, Y. P. *J. Compos. Mater.* **2011**, *45*, 2555.
33. Marcano, D. C.; Kosynkin, D. V.; Berlin, J. M.; Sinitskii, A.; Sun, Z.; Slesarev, A.; Alemany, L. B.; Lu, W.; Tour, J. M. *ACS Nano.* **2010**, *4*, 4806.
34. Florian, H. G.; Malte, H. G. W.; Bodo, F.; Schulte, K. *Compos. Sci. Technol.* **2005**, *65*, 2300.
35. Ramanathan, T.; Fisher, F. T.; Ruoff, R. S.; Brinson, L. C. *Chem. Mater.* **2005**, *17*, 1290.
36. Yoon, J. T.; Jeong, Y. G.; Lee, S. C.; Min, B. G. *Polym. Adv. Technol.* **2009**, *20*, 631.
37. Murariu, M.; Dechief, A.-L.; Paint, Y.; Peeterbroeck, S.; Bonnaud, L.; Dubois, P. *J. Polym. Environ.* **2012**, *20*, 932.
38. Aviles, F. *Express Polym. Lett.* **2011**, *5*, 766.
39. Katsoulis, C.; Kandare, E.; Kandola, B. K. *J. Fire Sci.* **2011**, *29*, 361.
40. Li, M.; Jeong, Y. G. *Compos. A: Appl. Sci. Manuf.* **2011**, *42*, 560.
41. Barrau, S.; Vanmansart, C.; Moreau, M.; Addad, A.; Stoclet, G.; Lefebvre, J. M.; Seguela, R. *Macromolecules* **2011**, *44*, 6496.